Supporting Information

for

Structurally screening of calixarenes as peptide transport activators

De-Yi Zhang[a], Zhe Zheng[a,b], Hong Zhao[a], Huan-Yu Wang[a], Fei Ding[a], Hua-Bin Li[a], Yu-Chen Pan[a]*, and Dong-Sheng Guo[a]*

[a] College of Chemistry, Key Laboratory of Functional Polymer Materials (Ministry of Education), State Key Laboratory of Elemento-Organic Chemistry, Tianjin Key Laboratory of Biosensing and Molecular Recognition, Nankai University, Tianjin 300071, P. R. China. E-mail: panyuchen@mail.nankai.edu.cn, dshguo@nankai.edu.cn

[b] School of Chemical Engineering & Technology, China University of Mining and Technology, Xuzhou 221000, Jiangsu, P. R. China

Table of contents

1. Materials

All reagents and solvents were commercially available and used as received unless otherwise specified purification. 5(6)-Carboxyfluorescein (CF) was purchased from Adamas Reagent Co. Ltd. Egg yolk phosphatidylcholine (EYPC) was purchased from Avanti Polar Lipids, Inc. Nonaarginine (Arg9) was purchased from Biosynthan. 1,6-Diphenyl-1,3,5-hexatriene (DPH) was purchased from Sigma-Aldrich, Inc. α-Poly-L-lysine (polyLys, degree of polymerization = 33) was purchased from Ark Pharm, Inc. Histones were purchased from Shanghai Yuanye Bio-Technology Co. Ltd. Two tripeptides (Ac-GKG-NH_2 and Ac-GRG-NH_2) were purchased from GL Biochem Ltd, and obtained in > 95 % purity as confirmed by HPLC and MS by the supplier. *p*-Sulfonatocalix[4]arene (sCx4),[1] *p*-sulfonatocalix[4]arene tetrahexyl ether (sCx4-6C),[2] *p*-sulfonatocalix[4]arene tetradodecyl ether (sCx4-12C), *p*-sulfonatocalix[5]arene pentaisohexyl ether (sCx5-6C),[3] *p*-sulfonatocalix[6]arene hexahexyl ether (sCx6-6C),[4] and *p*-sulfonatocalix[8]arene octahexyl ether (sCx8-6C)[2,5] were synthesized as reported. The synthetic methods of *p*-carboxycalix[5]arene pentaisohexyl ether (cCx5-6C) and *p*-phosphinocalix[5]arene pentaisohexyl ether (pCx5-6C) will be introduced in detail in section 3 (Schemes S1 and S2).

2. Instruments

^1H and ^{13}C nuclear magnetic resonance (NMR) data were recorded on a Bruker AV400 spectrometer or a Zhongke-Niujin BIXI-I 400 spectrometer. Mass spectrum was performed on a Varian ProMALDI and Bruker Daltonics AutoflexIII LRF200-CID spectrometer. The sample solutions for dynamic light scattering (DLS) were examined on a laser light scattering spectrometer (NanoBrook 173plus) equipped with a digital correlator at 659 nm at a scattering angle of 90°. The kinetic fluorescence traces and the fluorescence anisotropy were recorded in a conventional quartz cell (light path 10 mm) on a Varian Cary Eclipse spectrometer equipped with a Varian Automated Polarization accessory and a Varian Cary single-cell peltier accessory to control temperature and provide magnetic stirring.

3. Synthesis and characterization of calixarenes

3.1 Structures of calixarenes

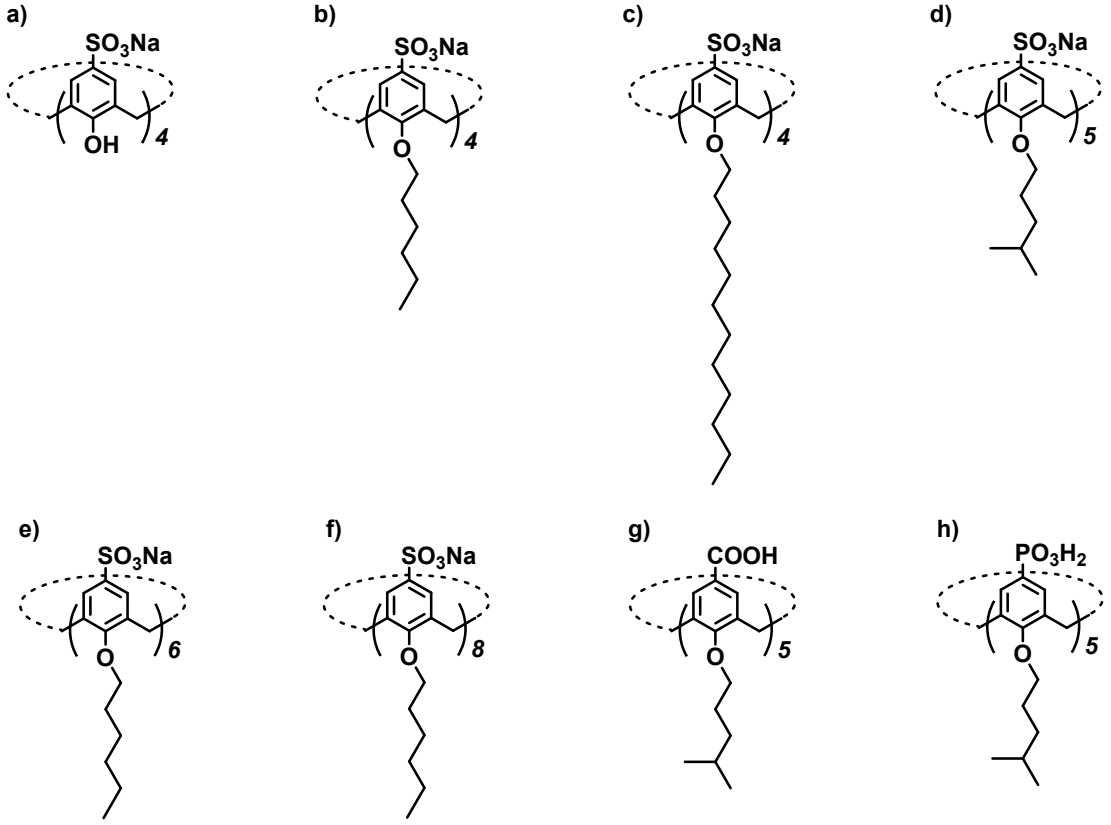

Figure S1. Chemical structures of a) sCx4, b) sCx4-6C, c) sCx4-12C, d) sCx5-6C, e) sCx6-6C, f) sCx8-6C, g) cCx5-6C, h) pCx5-6C.

3.2 Synthesis of cCx5-6C

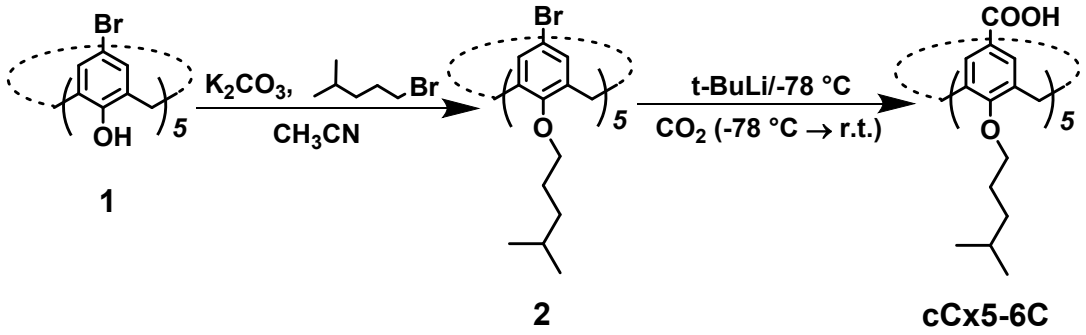

Scheme S1. Synthesis route of cCx5-6C.

cCx5-6C was synthesized as follows. Mixture of **1** (0.40 g, 0.43 mmol), K_2CO_3 (1.8 g, 13 mmol), and 1-bromo-4-methylpentane (1.28 mL, 8.6 mmol) in dry acetonitrile (30 mL) was stirred for 20 h at 65 °C. After cooling, the mixture was filtered, and the solid was washed with 80 mL chloroform. The combined filtrate was washed with dilute HCl, saturated brine and water and evaporated to dryness. The residue was stirred for 30 min in 30 mL of methanol. A pale yellow powder was obtained after filtration. The powder was dissolved in a minimum amount of dichloromethane and precipitated upon addition of methanol (20 mL). White powder **2** was obtained. To a solution of 500 mg (0.371 mmol) of **2** in 25 mL tetrahydrofuran (THF) under argon, 4.0 mL of t-butyl lithium (1.6 M, 6.4 mmol) dripped within 45 min at −78 °C under argon. The reaction mixture was stirred for 30 min, and then naturally heated up to −50 °C, and then kept for 3.5 h. An excess of CO_2 gas dried over P_2O_5 was bubbled through the mixture while the cooling was removed. After reaching room temperature, the mixture was quenched with water (10 mL) and acidified with 6 M HCl, and the pH was adjusted to 3-4. Using a separatory funnel, the aqueous phase was extracted three times with chloroform. All organic phase was then evaporated under vacuum. The precipitate was recrystallized from THF/acetone. White cCx5-6C was obtained. The characterization results of cCx5-6C are indicated as follows: ^{1}H NMR (400 MHz, tetrahydrofuran-d_8, δ): 7.64 (s, 10H; Ar-*H*), 4.59 (d, J = 14.17 Hz, 5H; Ar-C*H*$_2$-Ar), 3.85 (t, J = 7.32 Hz, 10H; Ar-O-C*H*$_2$), 3.46 (d, J = 14.32 Hz, 5H; Ar-C*H*$_2$-Ar), 1.94 (m, 10H; O-CH$_2$-C*H*$_2$), 1.64 (m, 5H; C*H*-(CH$_3$)$_2$), 1.35 (m, 10H; C*H*$_2$-CH-(CH$_3$)$_2$), 0.96 (d, J = 6.56 Hz, 30H; C*H*$_3$). ^{13}C NMR (100 MHz, tetrahydrofuran-d_8, δ): 167.49, 159.48, 134.39, 131.25, 126.56, 74.67, 35.90, 30.67, 28.98, 28.90, 23.01. Mass spectrum (MALDI-TOF) m/z: [M + Li]$^+$ calcd. for $C_{70}H_{90}O_{15}Li^+$ 1177.6435, found 1177.6577; [M + Na]$^+$ calcd. for $C_{70}H_{90}O_{15}Na^+$ 1193.6172, found 1193.6175; [M + K]$^+$ calcd. for $C_{70}H_{90}O_{15}K^+$ 1209.5912, found 1209.5918.

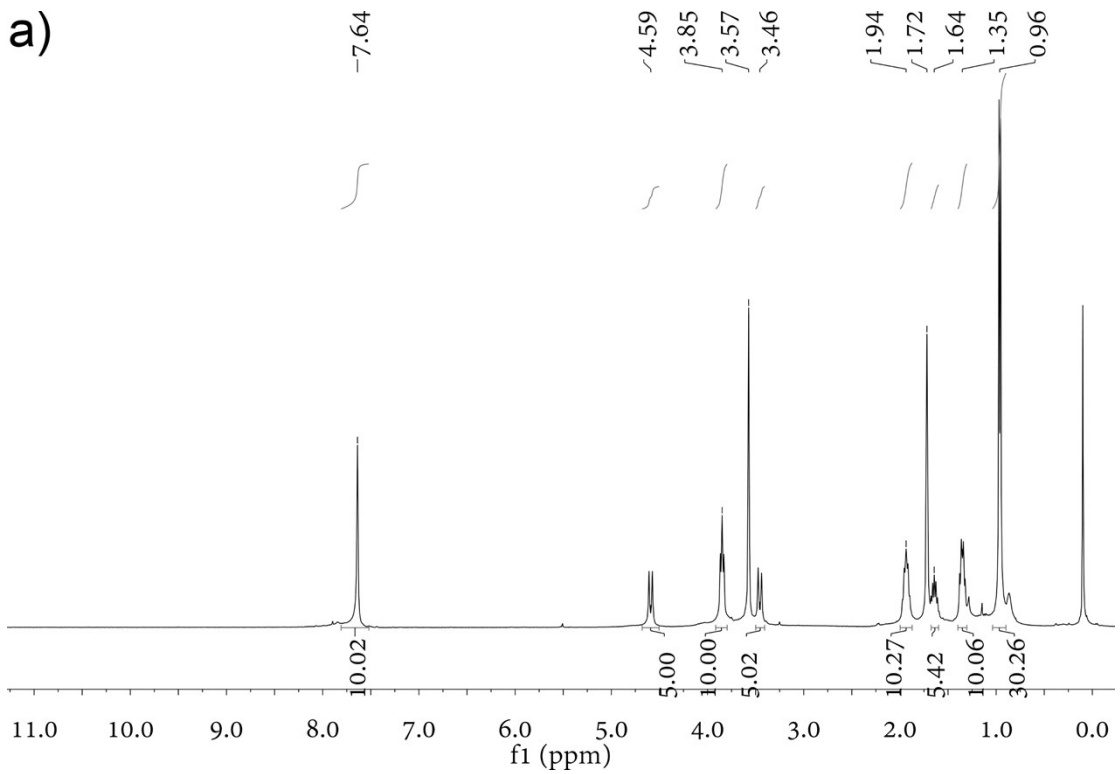
a)
7.64
4.59
3.85
3.57
3.46
1.94
1.72
1.64
1.35
0.96
10.02
5.00
10.00
5.02
10.27
5.42
10.06
30.26
11.0 10.0 9.0 8.0 7.0 6.0 5.0 4.0 3.0 2.0 1.0 0.0
f1 (ppm)

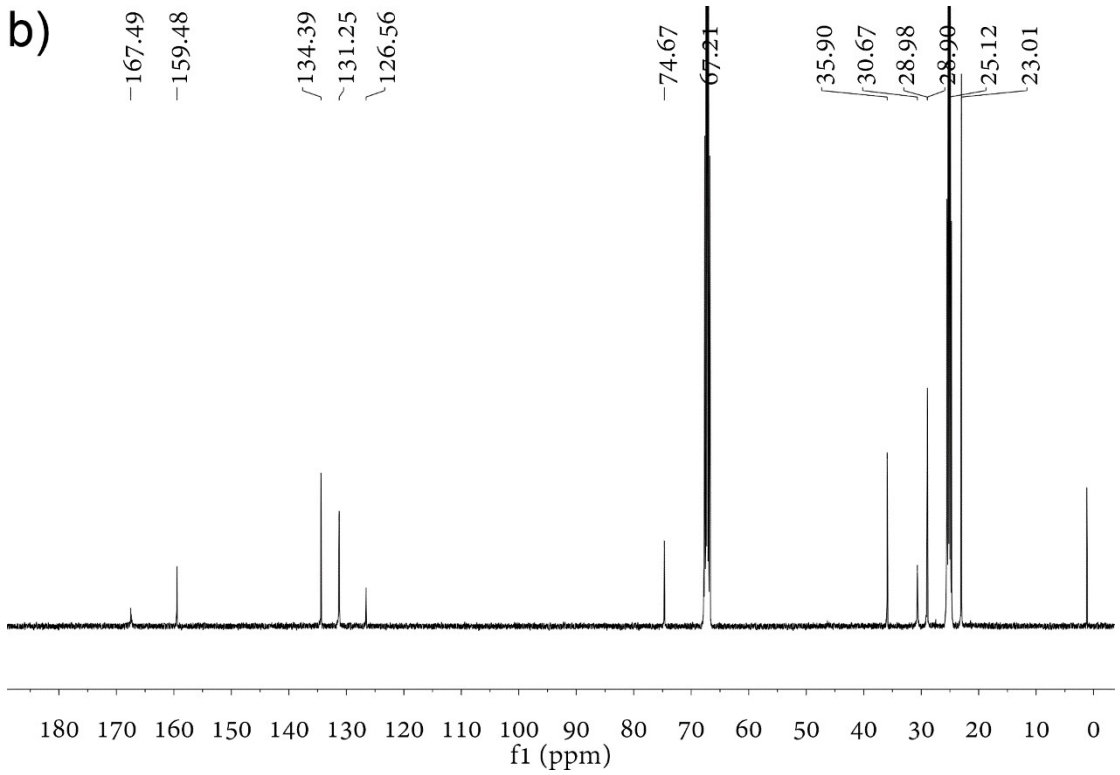
b)
167.49
159.48
134.39
131.25
126.56
74.67
67.21
35.90
30.67
28.98
28.90
25.12
23.01
180 170 160 150 140 130 120 110 100 90 80 70 60 50 40 30 20 10 0
f1 (ppm)

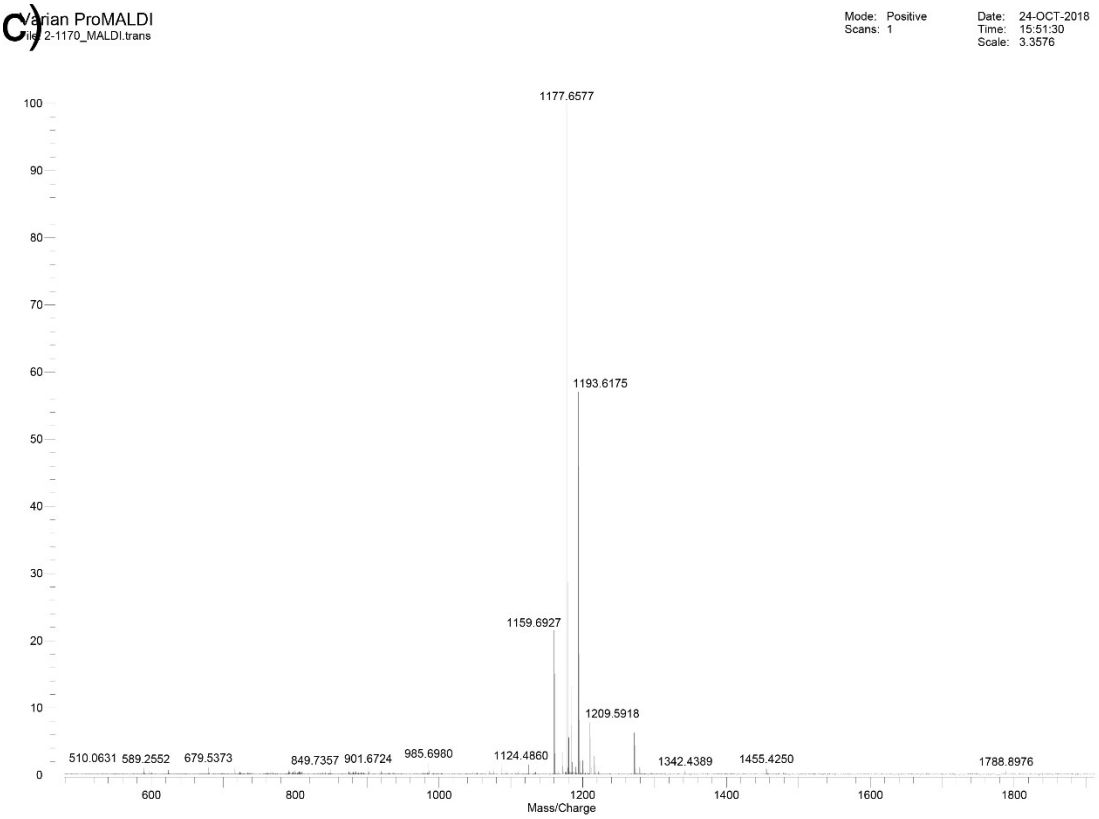

Figure S2. a) ^{1}H NMR spectrum of cCx5-6C in tetrahydrofuran-d_8, 400 MHz, 25 °C; b) ^{13}C NMR spectrum of cCx5-6C in tetrahydrofuran-d_8, 100 MHz, 25 °C; c) Mass spectrum (MALDI-TOF) of cCx5-6C.

3.3 Synthesis pCx5-6C

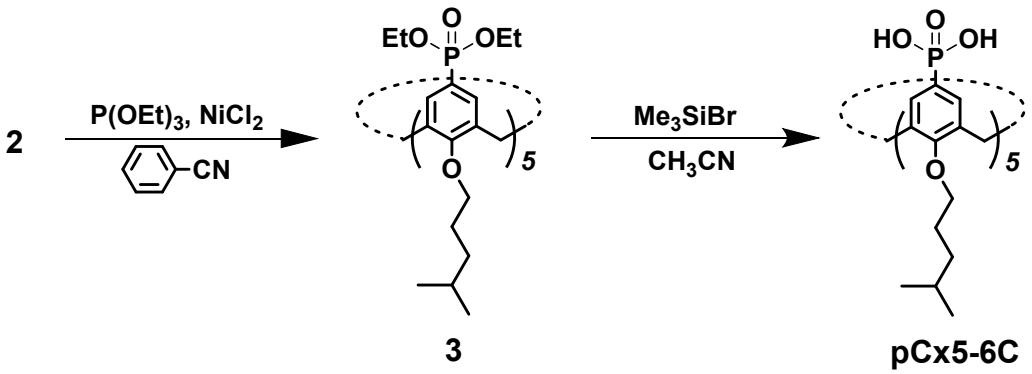

Scheme S2. Synthesis route of pCx5-6C.

pCx5-6C was synthesized as follows. Compound **2** (1.076 g, 0.799 mmol), $P(OEt)_3$ (1.36 mL, 7.88 mmol), $NiCl_2$ (103.6 mg, 0.810 mmol) were added into benzonitrile (8.0 mL) and reacted for 3 h. The reaction result was monitored by thin layer chromatography with a ratio of CH_2Cl_2 : CH_3OH = 20 : 1, and it was found that four points including the raw material were included. The product then ran on an alkaline pillar chromatography, and the final forth point which was compound **3** was collected. Compound **3** (249.67 mg, 0.153 mmol), Me_3SiBr (0.40 mL, 3.06 mmol) and chromatographically pure CH_3CN (2.3 mL) were added to the reaction flask and refluxed for 16 h. After the reaction, the solvent was rotary evaporated. After washing with CH_3CN (4.0 mL) + H_2O (0.200 mL), a solid which was pCx5-6C (145 mg) precipitated out. The characterization results of pCx5-6C are indicated as follows: ^{1}H NMR (400 MHz, CD_3OD, δ): 7.45 (d, J = 13.61 Hz, 10H; Ar-*H*), 4.64 (d, J = 14.11 Hz, 5H; Ar-CH_2-Ar), 3.90 (t, J = 7.38 Hz, 10H; Ar-O-CH_2), 3.50 (d, J = 14.23 Hz, 5H; Ar-CH_2-Ar), 1.96 (m, 10H; O-CH_2-CH_2), 1.65 (m, 5H; C*H*-$(CH_3)_2$), 1.39 (m, 10H; CH_2-CH-$(CH_3)_2$), 0.98 (d, J = 6.64 Hz, 30H; CH_3). ^{13}C NMR (100 MHz, CD_3OD, δ): 159.51, 135.49, 133.01, 128.35, 126.49, 75.54, 36.44, 30.88, 29.40, 23.28. Mass spectrum (MALDI-TOF) m/z: $[M + H]^+$ calcd. $C_{65}H_{96}O_{20}P_5^+$ 1351.51, found 1351.42.

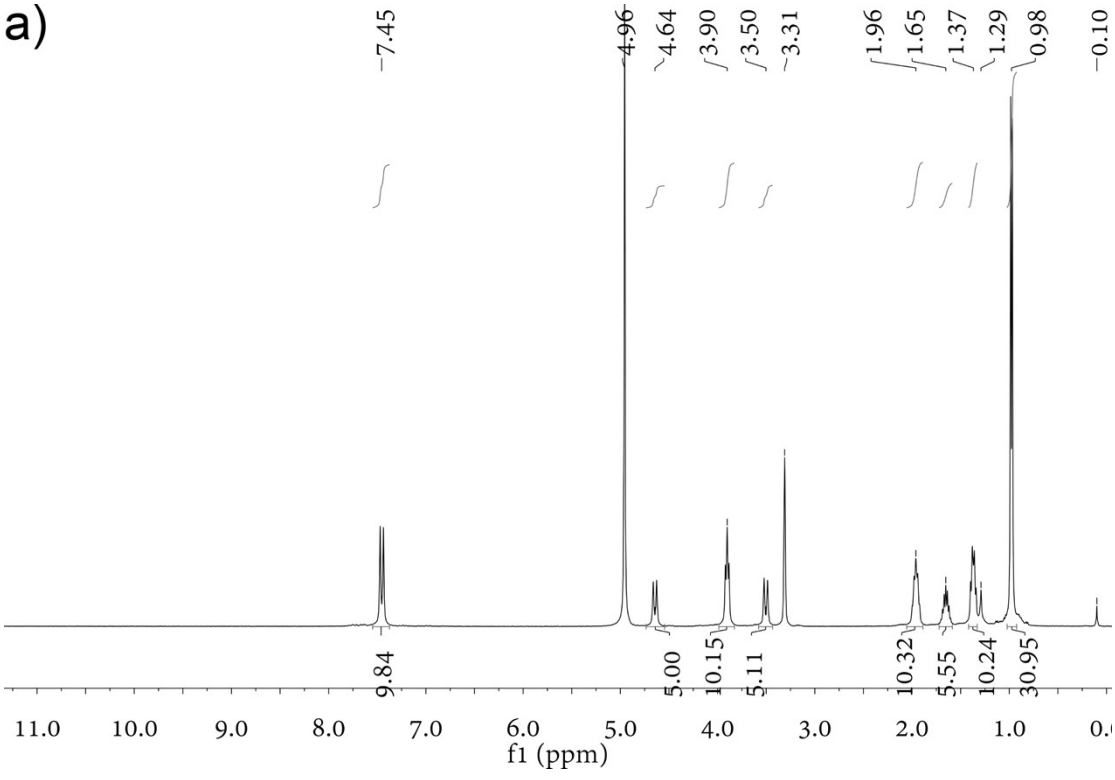

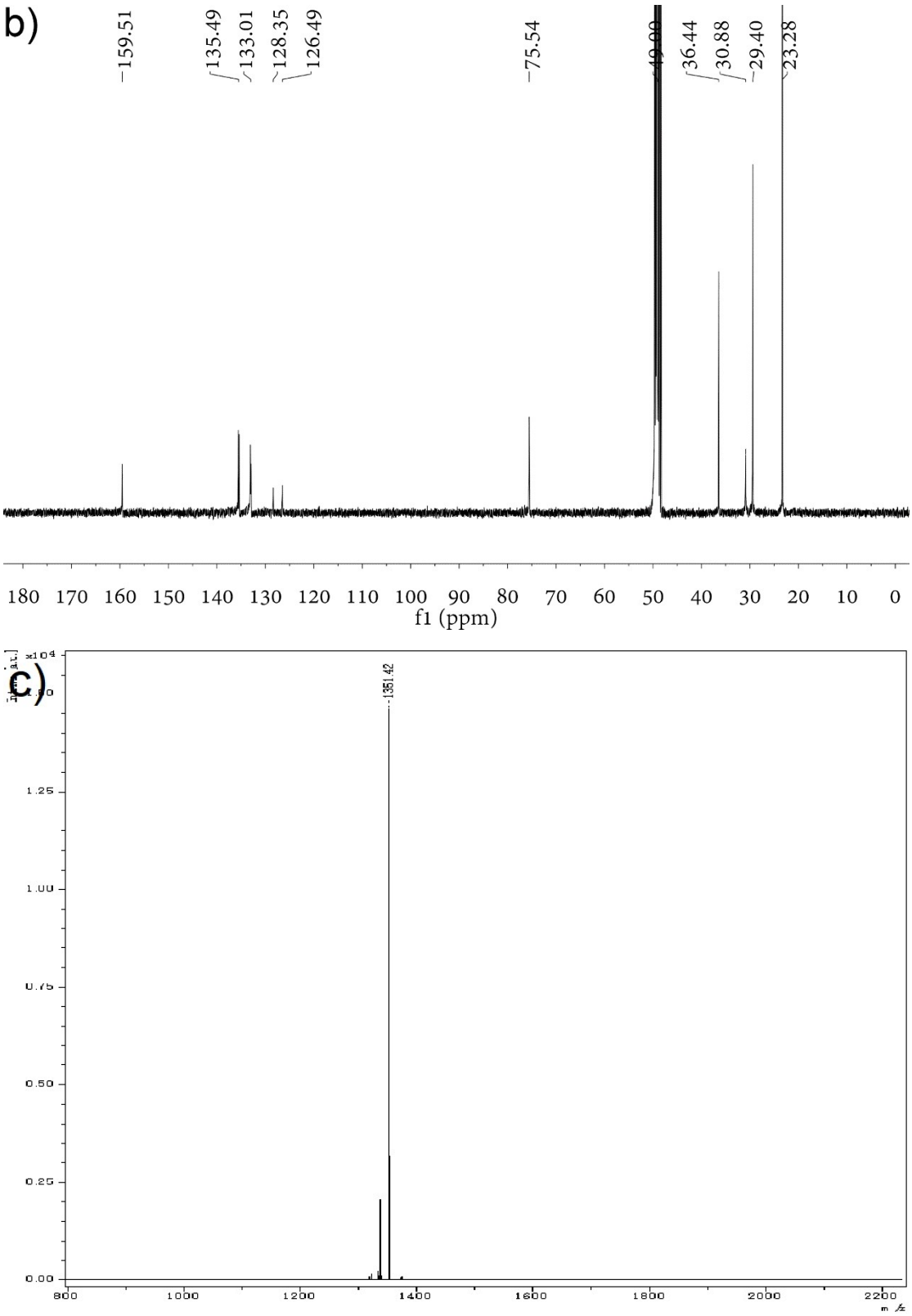

Figure S3. a) ^{1}H NMR spectrum of pCx5-6C in CD_3OD, 400 MHz, 25 °C; b) ^{13}C NMR spectrum of pCx5-6C in CD_3OD, 100 MHz, 25 °C; c) Mass spectrum (MALDI-TOF) of pCx5-6C.

3.4 ^{1}H NMR of sCx4, sCx4-6C, sCx4-12C, sCx5-6C, sCx6-6C, and sCx8-6C

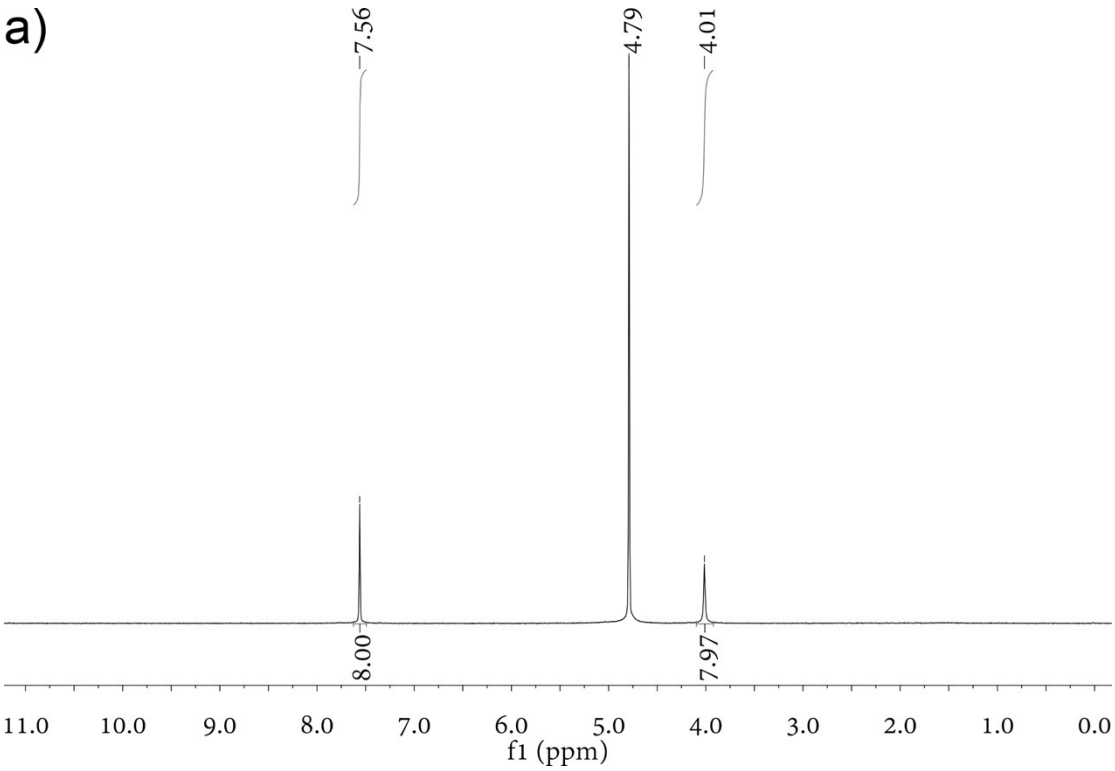

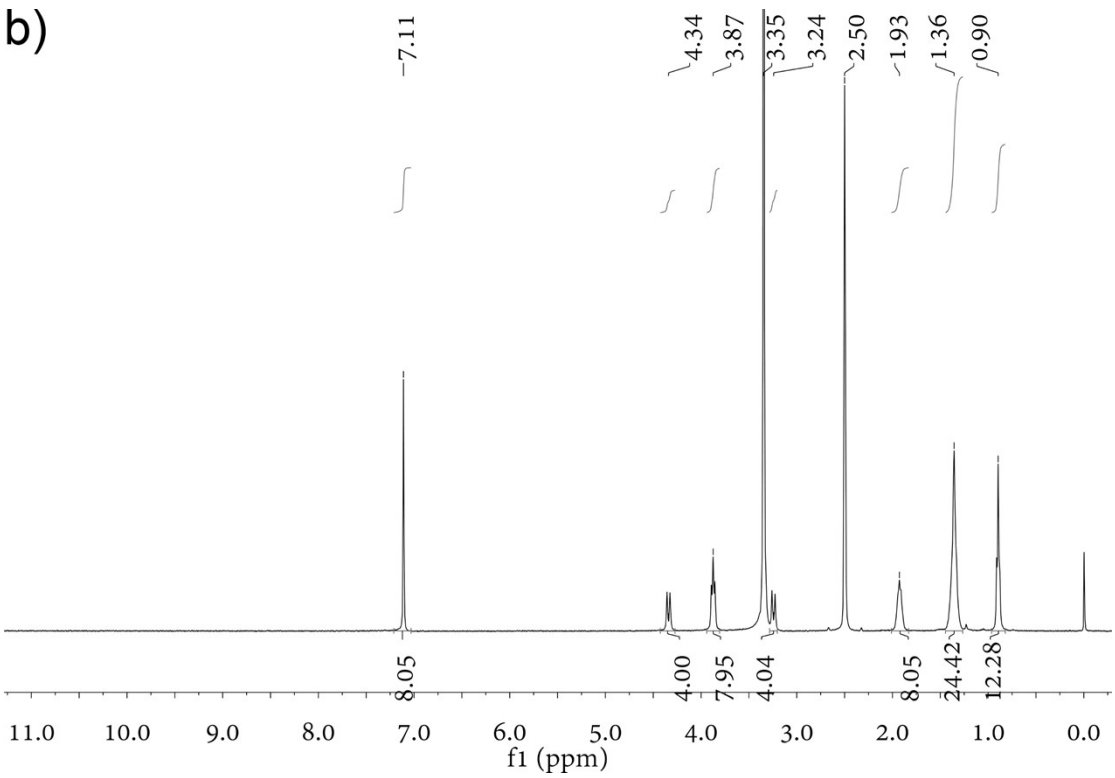

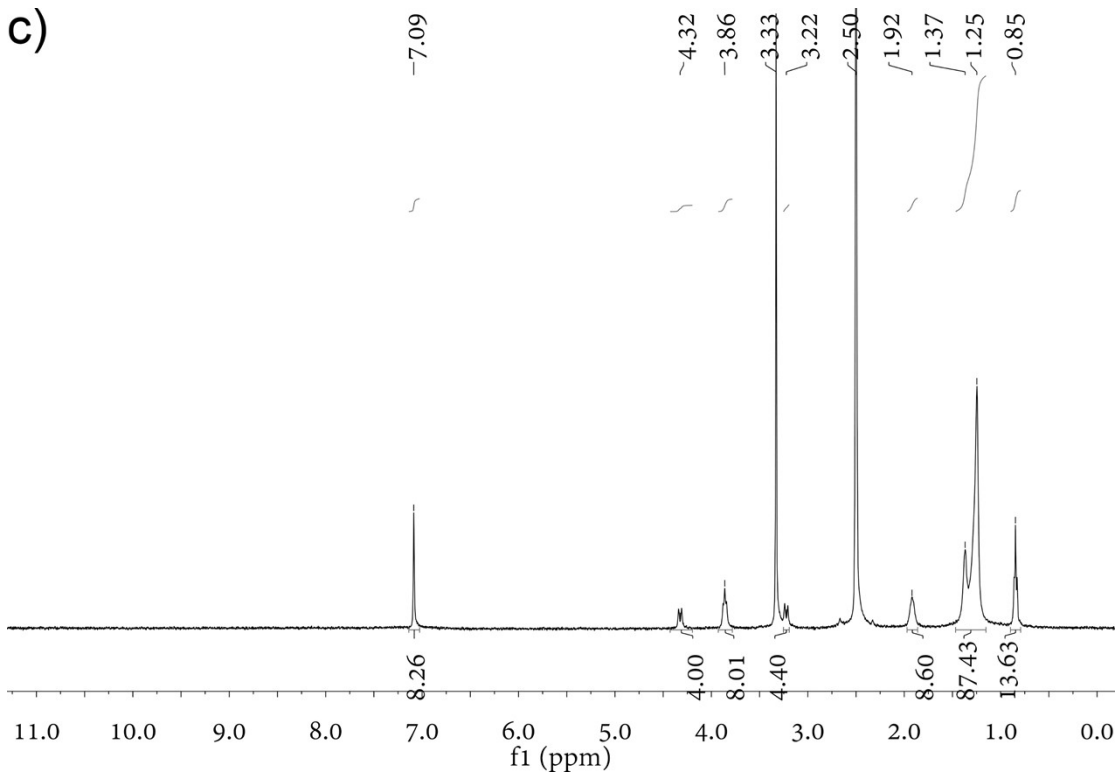
c)
7.09
4.32
3.86
3.33
3.22
2.50
1.92
1.37
1.25
0.85
8.26
4.00
8.01
4.40
8.60
87.43
13.63
11.0 10.0 9.0 8.0 7.0 6.0 5.0 4.0 3.0 2.0 1.0 0.0
f1 (ppm)

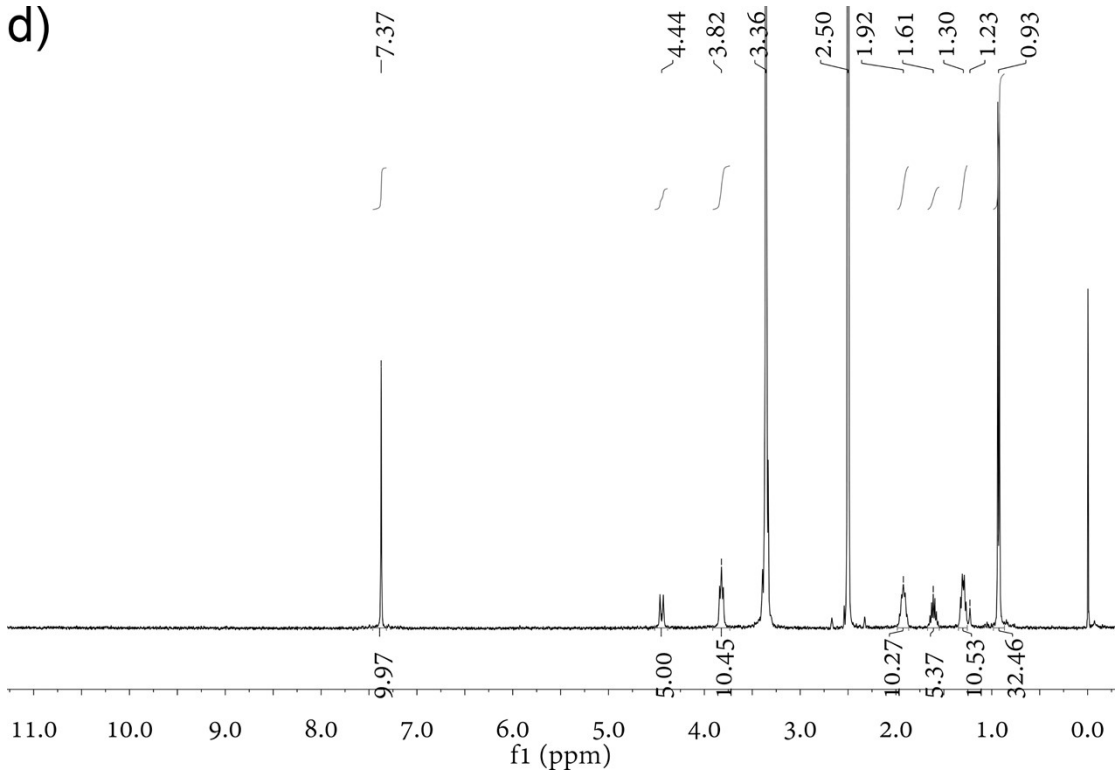
d)
7.37
4.44
3.82
3.36
2.50
1.92
1.61
1.30
1.23
0.93
9.97
5.00
10.45
10.27
5.37
10.53
32.46
11.0 10.0 9.0 8.0 7.0 6.0 5.0 4.0 3.0 2.0 1.0 0.0
f1 (ppm)

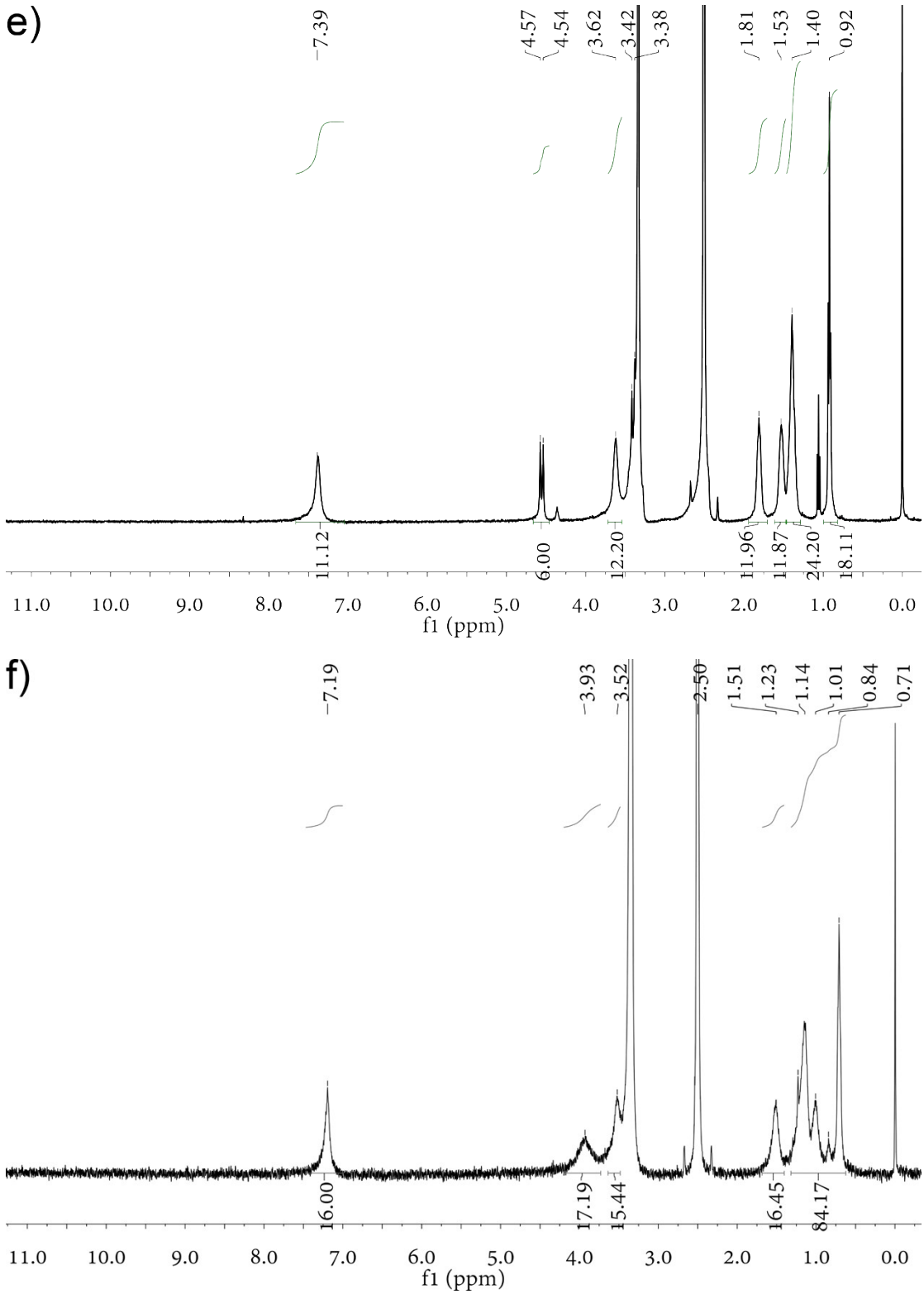

Figure S4. ^{1}H NMR spectrum (400 MHz, 25 °C) of a) sCx4 in D_2O, b) sCx4-6C in DMSO-d_6, c) sCx4-12C in DMSO-d_6, d) sCx5-6C in DMSO-d_6, e) sCx6-6C in DMSO-d_6, and f) sCx8-6C in DMSO-d_6.

4. Method

All mean values from fluorescence anisotropy and fluorescence titrations were measured from at least two experiments and errors were given as standard deviation ($\pm 1\sigma$). Data are presented as mean ± s.d..

4.1 Preparation of large unilamellar vesicles

EYPC large unilamellar vesicles (EYPC-LUVs): EYPC in chloroform (0.500 mL 25.0 mg/mL) was dried in a stream of nitrogen and then dried in vacuo overnight. The lipid film was rehydrated with 0.500 mL 10 mM HEPES, pH 7.4 by agitation at room temperature for 30 min. The suspension was subjected to 5 freeze-thaw cycles and 15 extrusions through a polycarbonate membrane (pore size = 100 nm). Vesicle size was confirmed by DLS. Phospholipid concentration was determined by Stewart assay.[6]

CF-encapsulated EYPC-LUVs (EYPC-LUVs⊃CF): EYPC in chloroform (0.500 mL 25.0 mg/mL) was dried in a stream of nitrogen and then dried in vacuo overnight. The lipid film was rehydrated with 0.500 mL 10 mM HEPES, 50 mM CF, pH 7.4 by agitation at room temperature for 30 min. The suspension was subjected to 5 freeze-thaw cycles and 15 extrusions through a polycarbonate membrane (pore size = 100 nm). Extravesicular components were removed by size exclusion chromatography (NAP-25 column) with 10 mM HEPES, 107 mM NaCl, pH 7.4. Vesicle size was confirmed by DLS. Phospholipid concentration was determined by Stewart assay.[6]

4.2 Fluorescence anisotropy measurements

DPH loaded vesicle solutions were prepared by the following method. The solutions of DPH in chloroform were dried in vacuo. Then a certain amount of EYPC-LUVs solution, HEPES (10 mM, pH 7.4) buffer and a series of concentrations of calixarenes were added until got a mixed solution with 50.0 μM EYPC-LUVs, 1 μM DPH and expected concentration of calixarenes. The samples were sonicated at 80 °C for 60 min, subsequently cooled to room temperature. The samples were excited with vertically polarized light (360 nm), and emission intensities both perpendicular and

parallel to the excitation light were recorded at 430 nm.

4.3 Transport assays

CF assay: The CF assay relies on high local concentrations of CF inside the vesicle such that the fluorescence is quenched.[7] The translocation of CF to the outside of vesicle leads to dilution of the CF. Consequently, quenching no longer applies and the transport activity is signaled as fluorescence recovery. The experiment operation is as follows: the EYPC-LUVs⊃CF stock solution was diluted with 10 mM HEPES, 107 mM NaCl, pH 7.4 to 10.0 μM in a quartz cuvette and the time-dependent change in the fluorescence intensity, I_t, was monitored (λ_{ex} = 492 nm, λ_{em} = 517 nm) during addition of ≤ 20.0 μL activator in DMSO at 60 s, ≤ 10.0 μL peptide in water at 120 s and 60.0 μL 1.2 % (wt/vol) Triton X-100 (TX-100) in water (for vesicle lysis and calibration) at 600 s. Time courses of I_t were normalized to fractional intensities, I_f, using the equation (1), where $I_0 = I_t$ before peptides addition and $I_\infty = I_t$ after lysis. For Hill analysis, I_f before lysis was defined as transmembrane activity, Y, and plotted against concentrations of activator, c, and fitted to the Hill equation (equation (2)) to afford the transmembrane activity in absence of activator, Y_0, the maximal transmembrane activity, Y_{max}, the effective concentration needed to reach $Y_{max}/2$, EC_{50}, and the Hill coefficient, n. The activation efficiency, E, was defined in equation (3) to reflect Y_{max} and EC_{50} simultaneously.[8,9] pEC_{50} is the negative logarithm of EC_{50} and f is an arbitrary scaling factor set to 20.6 in this study.

$$I_f = \frac{I_t - I_0}{I_\infty - I_0} \#(1)$$

$$Y = Y_0 + \frac{Y_{max} - Y_0}{1 + \left(\frac{EC_{50}}{c}\right)^n} \#(2)$$

$$E = Y_{max} \times \frac{pEC_{50}}{f} \#(3)$$

Screening appropriate concentrations of Arg9 and polyLys as peptides: The purpose of this work is to effectively transport by calixarenes. Therefore, we firstly

fixed the concentration of calixarenes, and screened out the appropriate concentration of Arg9 or polyLys. Then we fixed the Arg9 or polyLys at the appropriate concentration and studied the transport efficiency activated by calixarenes. To screen the appropriate Arg9 or polyLys concentration, the concentration of the calixarene was fixed (0.200 μM) and the transport activities were monitored as a function of concentration of Arg9 or polyLys. The Arg9 or polyLys concentration, at which most calixarenes obtained a high *Y* value, was chosen as the appropriate concentration and used for the subsequent experiments.

5. Supporting results

5.1 DLS measurement

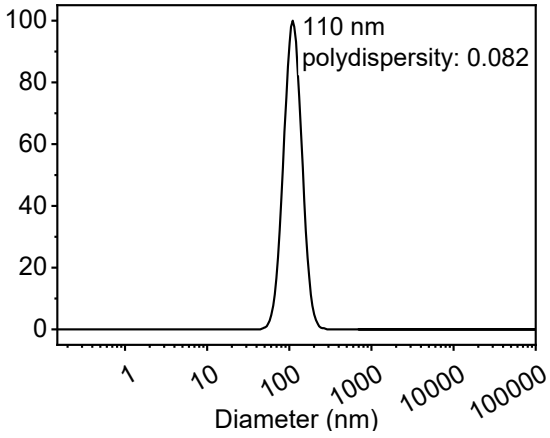

Figure S5. DLS data of the EYPC-LUVs⊃CF in 10 mM HEPES buffer (pH = 7.4, [EYPC-LUVs⊃CF] = 10.0 μM).

5.2 Results of CF assays

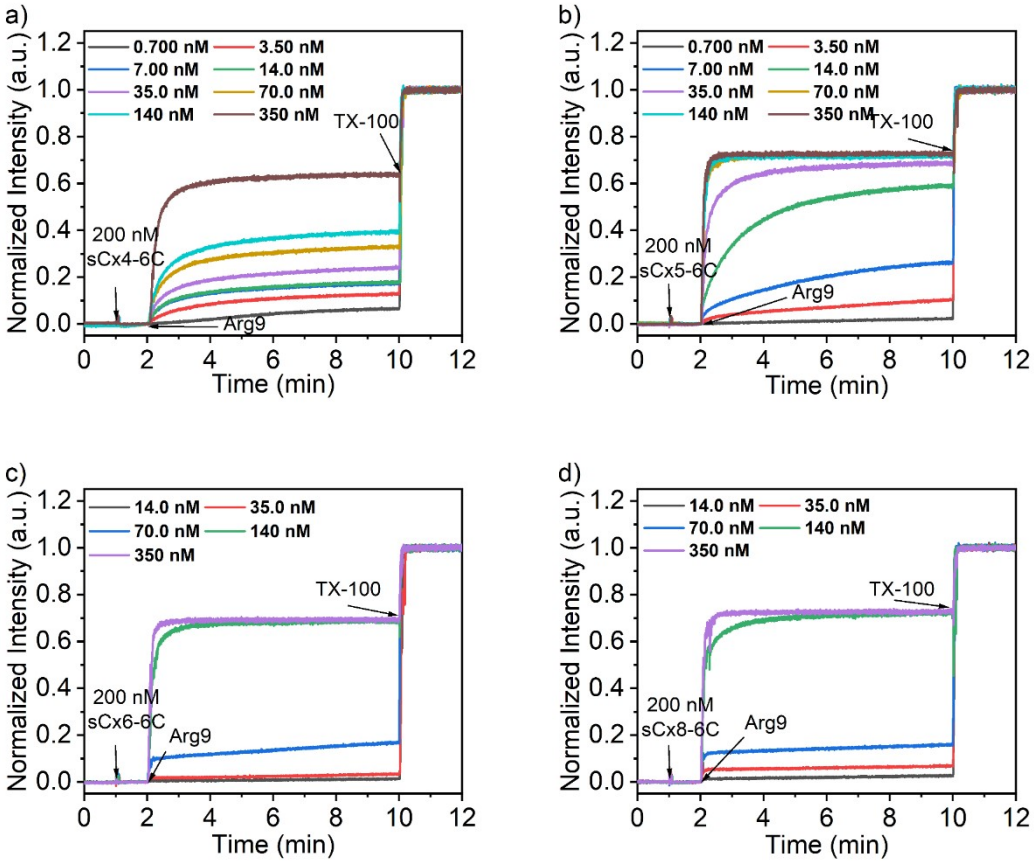

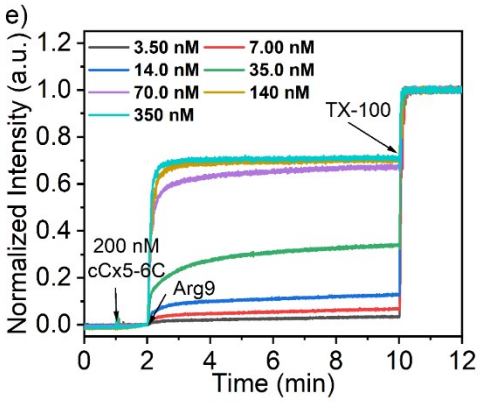
e)
Normalized Intensity (a.u.)
Time (min)
3.50 nM
7.00 nM
14.0 nM
35.0 nM
70.0 nM
140 nM
350 nM
TX-100
200 nM
cCx5-6C
Arg9

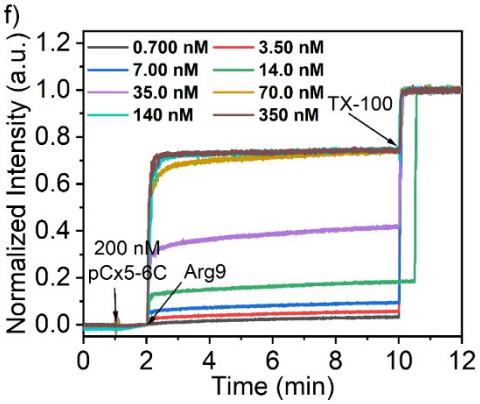
f)
Normalized Intensity (a.u.)
Time (min)
0.700 nM
3.50 nM
7.00 nM
14.0 nM
35.0 nM
70.0 nM
140 nM
350 nM
TX-100
200 nM
pCx5-6C
Arg9

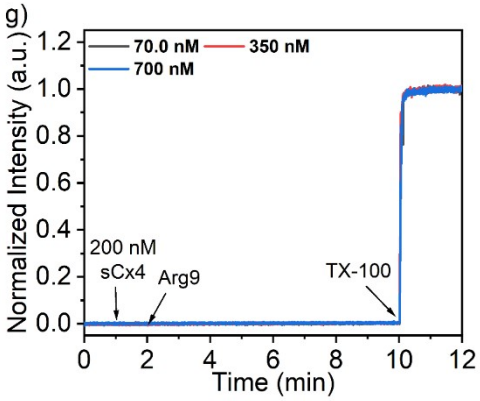
g)
Normalized Intensity (a.u.)
Time (min)
70.0 nM
350 nM
700 nM
200 nM
sCx4
Arg9
TX-100

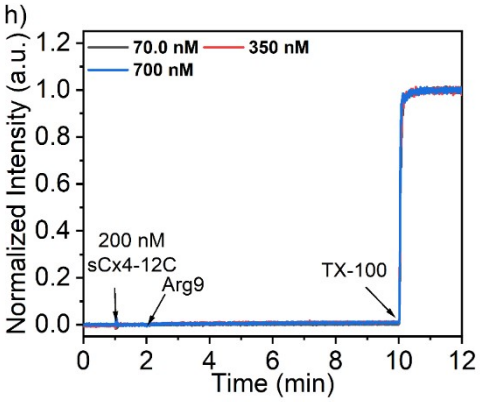
h)
Normalized Intensity (a.u.)
Time (min)
70.0 nM
350 nM
700 nM
200 nM
sCx4-12C
Arg9
TX-100

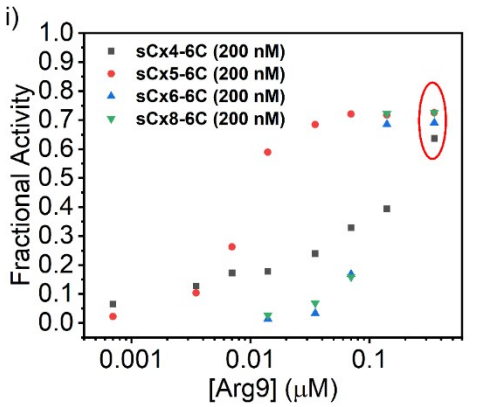
i)
Fractional Activity
[Arg9] (μM)
sCx4-6C (200 nM)
sCx5-6C (200 nM)
sCx6-6C (200 nM)
sCx8-6C (200 nM)

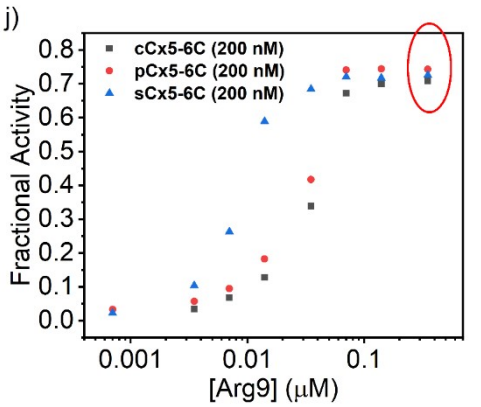
j)
Fractional Activity
[Arg9] (μM)
cCx5-6C (200 nM)
pCx5-6C (200 nM)
sCx5-6C (200 nM)

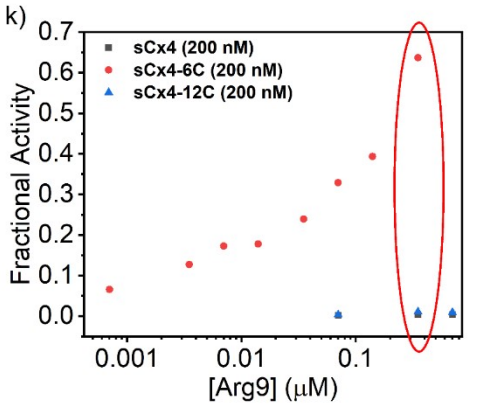
k)
Fractional Activity
[Arg9] (μM)
sCx4 (200 nM)
sCx4-6C (200 nM)
sCx4-12C (200 nM)

Figure S6. Dependence of transport activities on concentration of Arg9. Changes in fractional CF emission intensity (λ_{ex} = 492 nm, λ_{em} = 517 nm) were monitored in real time upon addition of 200 nM a) sCx4-6C, b) sCx5-6C, c) sCx6-6C, d) sCx8-6C, e) cCx5-6C, f) pCx5-6C, g) sCx4 and h) sCx4-12C, varying concentrations of Arg9, and TX-100 (for calibration) to 10.0 μM EYPC-LUVs⊃CF in 10 mM HEPES, 107 mM NaCl, pH 7.4, 25 °C. i) Activation efficiencies of sCx4-6C, sCx5-6C, sCx6-6C and sCx8-6C by varying concentrations of Arg9. j) Activation efficiencies of sCx5-6C, cCx5-6C and pCx5-6C by varying concentrations of Arg9. k) Activation efficiencies of sCx4, sCx4-6C and sCx4-12C by varying concentrations of Arg9. The selected Arg9 concentration (0.350 μM) is marked in red circles.

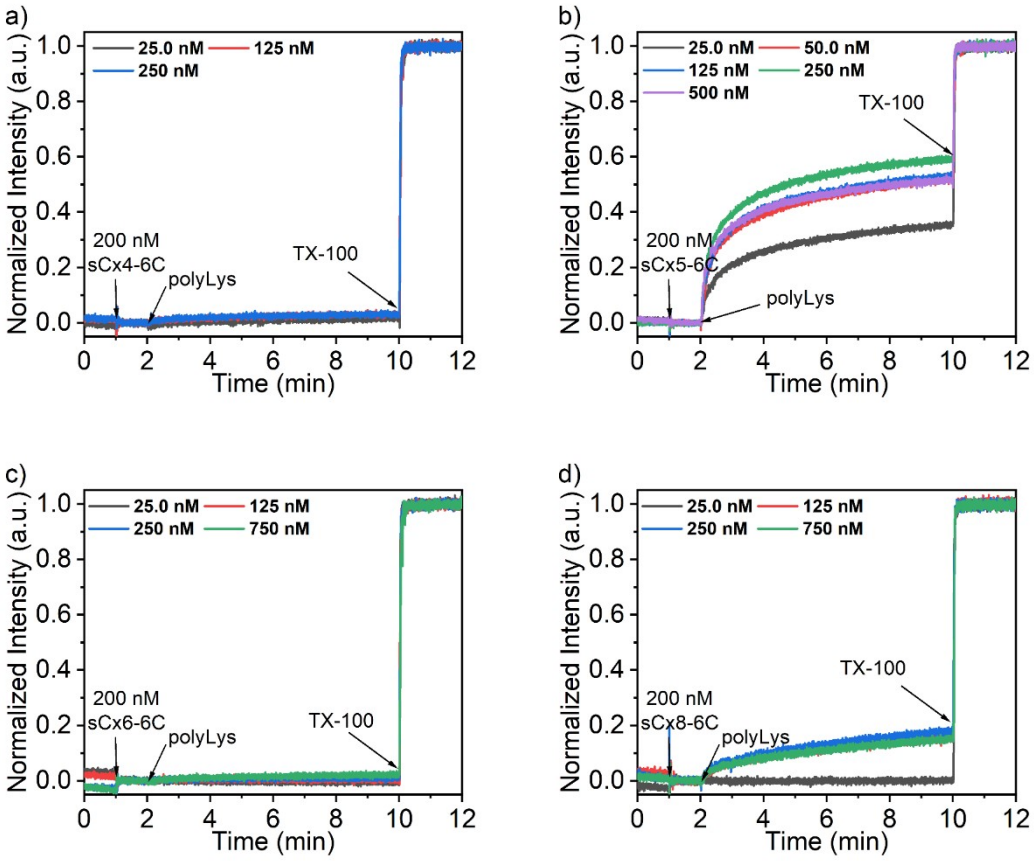

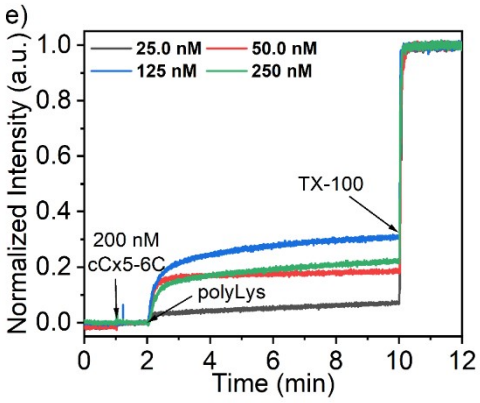
e)
Normalized Intensity (a.u.)
25.0 nM
50.0 nM
125 nM
250 nM
TX-100
200 nM
cCx5-6C
polyLys
Time (min)

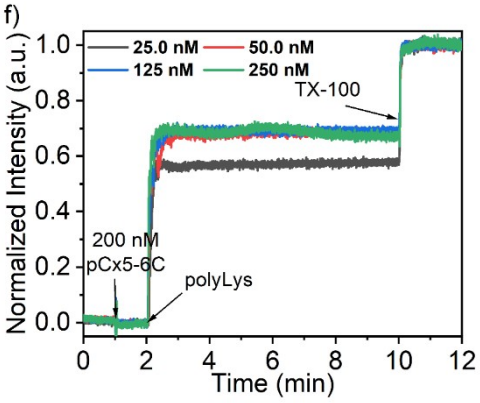
f)
Normalized Intensity (a.u.)
25.0 nM
50.0 nM
125 nM
250 nM
TX-100
200 nM
pCx5-6C
polyLys
Time (min)

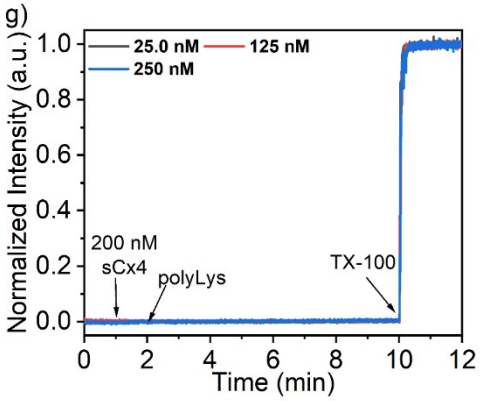
g)
Normalized Intensity (a.u.)
25.0 nM
125 nM
250 nM
200 nM
sCx4
polyLys
TX-100
Time (min)

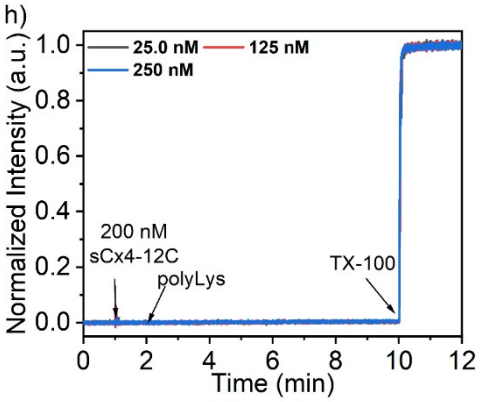
h)
Normalized Intensity (a.u.)
25.0 nM
125 nM
250 nM
200 nM
sCx4-12C
polyLys
TX-100
Time (min)

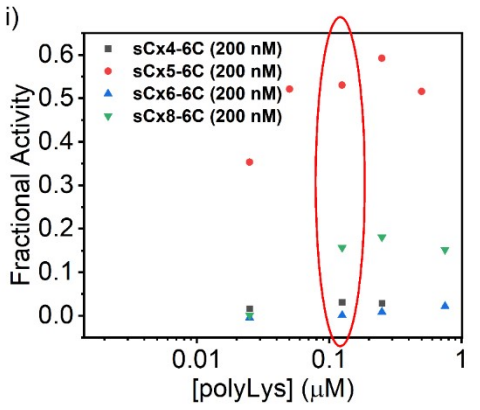
i)
Fractional Activity
sCx4-6C (200 nM)
sCx5-6C (200 nM)
sCx6-6C (200 nM)
sCx8-6C (200 nM)
[polyLys] (μM)

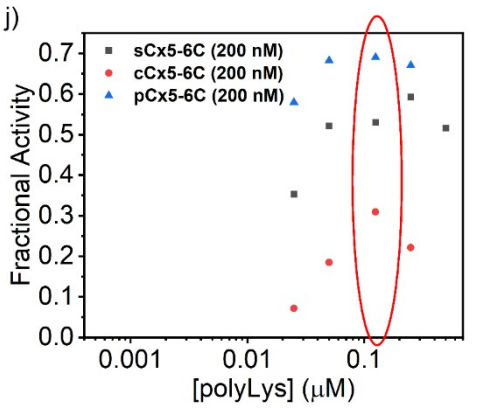
j)
Fractional Activity
sCx5-6C (200 nM)
cCx5-6C (200 nM)
pCx5-6C (200 nM)
[polyLys] (μM)

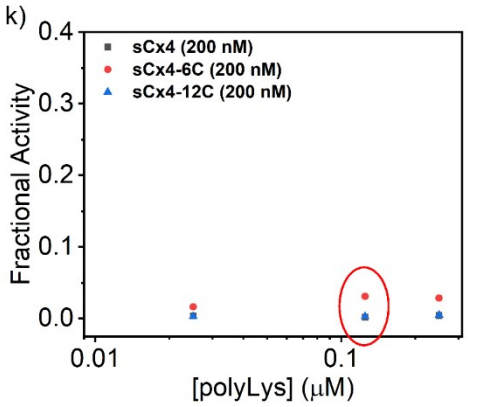
k)
Fractional Activity
sCx4 (200 nM)
sCx4-6C (200 nM)
sCx4-12C (200 nM)
[polyLys] (μM)

Figure S7. Dependence of transport activities on concentration of polyLys. Changes in fractional CF emission intensity (λ_{ex} = 492 nm, λ_{em} = 517 nm) were monitored in real time upon addition of 200 nM a) sCx4-6C, b) sCx5-6C, c) sCx6-6C, d) sCx8-6C, e) cCx5-6C, f) pCx5-6C, g) sCx4, and h) sCx4-12C, varying concentrations of polyLys, and TX-100 (for calibration) to 10.0 μM EYPC-LUVs⊃CF in 10 mM HEPES, 107 mM NaCl, pH 7.4, 25 °C. i) Activation efficiencies of sCx4-6C, sCx5-6C, sCx6-6C and sCx8-6C by varying concentrations of polyLys. j) Activation efficiencies of sCx5-6C, cCx5-6C and pCx5-6C by varying concentrations of polyLys. k) Activation efficiencies of sCx4, sCx4-6C and sCx4-12C by varying concentrations of polyLys. The selected polyLys concentration (0.125 μM) is marked in red circles.

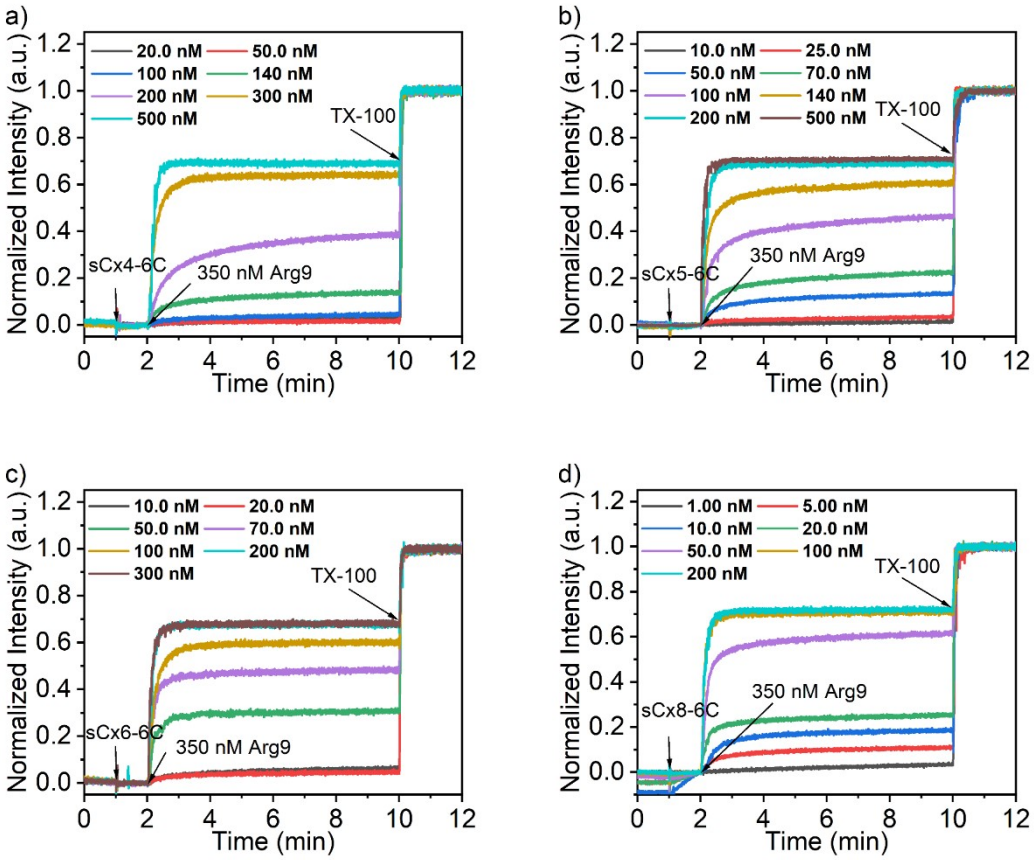

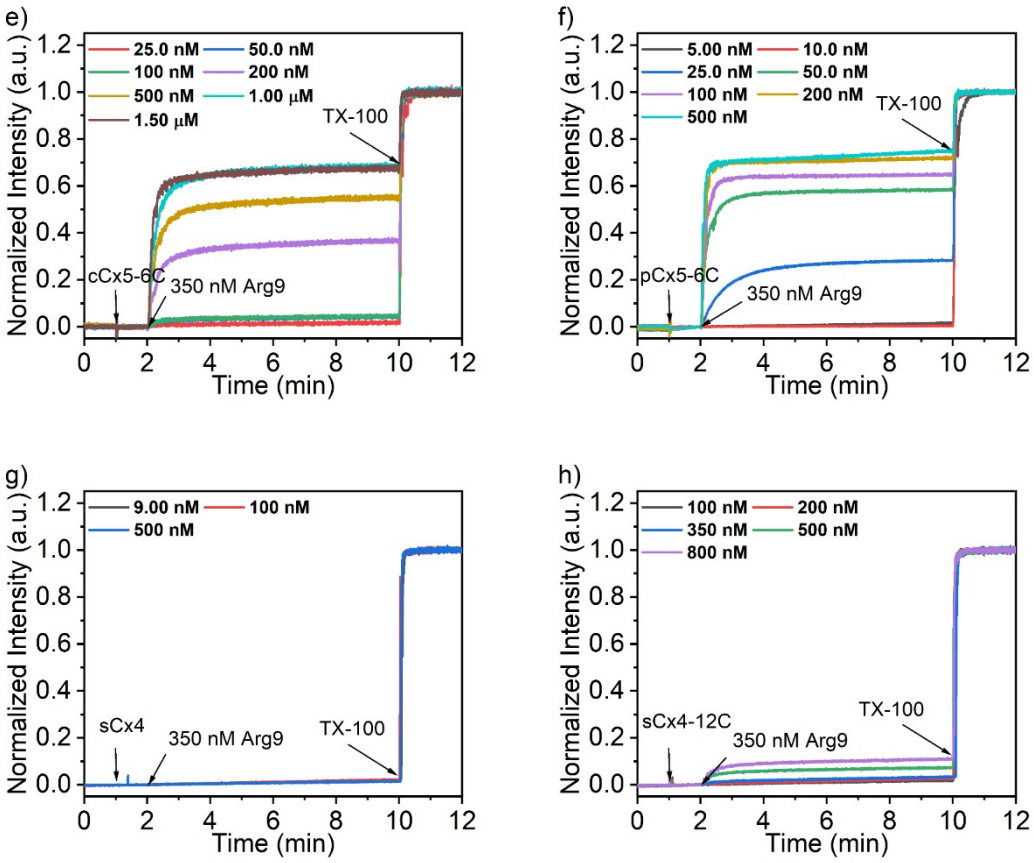

Figure S8. Dependence of Arg9 transport activities on concentration of a) sCx4-6C, b) sCx5-6C, c) sCx6-6C, d) sCx8-6C, e) cCx5-6C, f) pCx5-6C, g) sCx4, and h) sCx4-12C. Changes in fractional CF emission intensity (λ_{ex} = 492 nm, λ_{em} = 517 nm) were monitored in real time upon addition of varying concentrations of calixarenes, 0.350 μM Arg9, and TX-100 (for calibration) to 10.0 μM EYPC-LUVs⊃CF in 10 mM HEPES, 107 mM NaCl, pH 7.4, 25 °C.

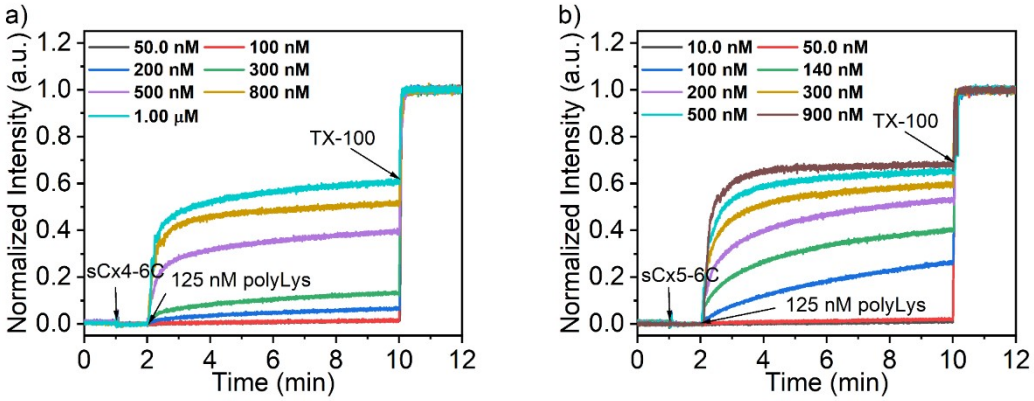

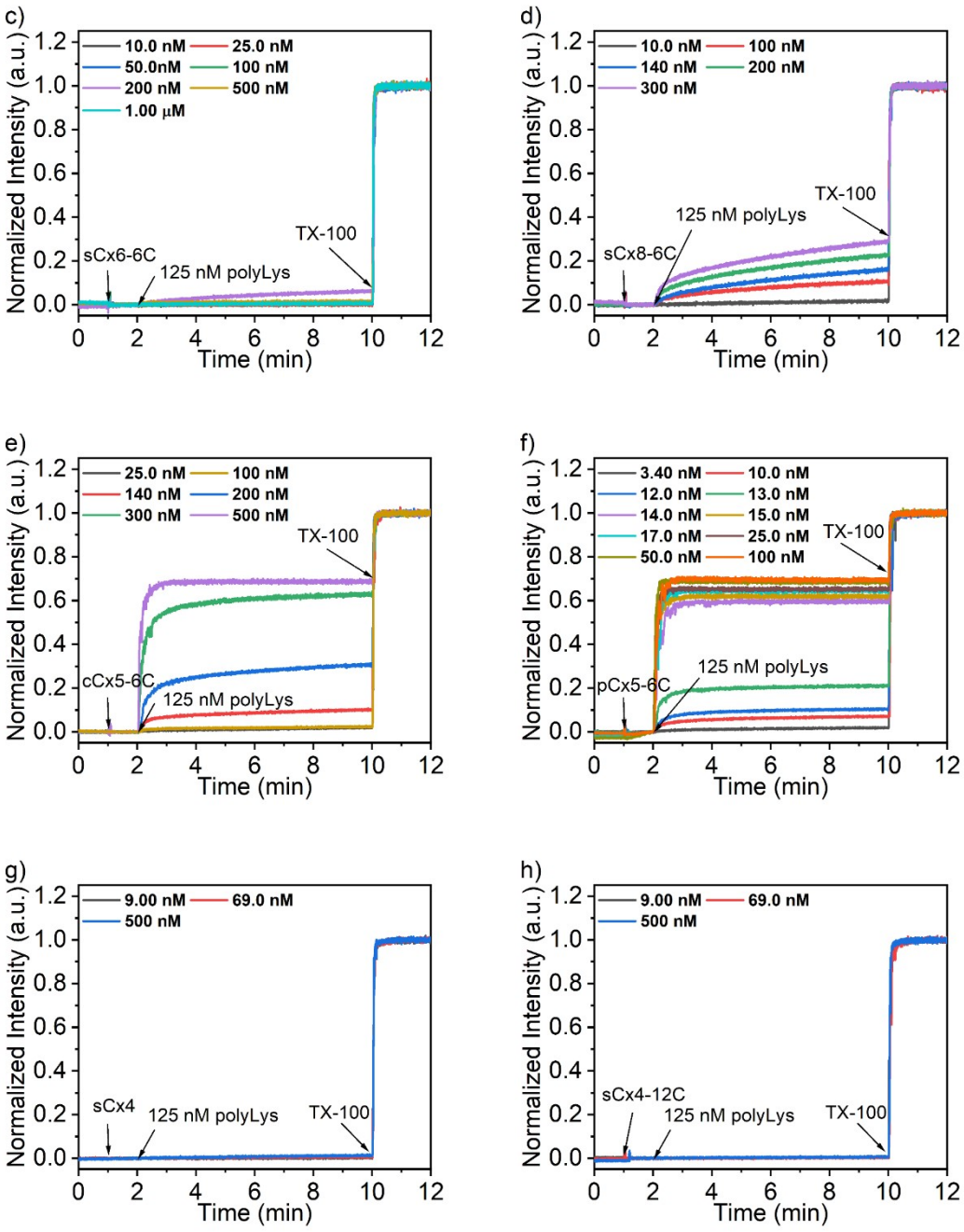

Figure S9. Dependence of polyLys transport activities on concentration of a) sCx4-6C, b) sCx5-6C, c) sCx6-6C, d) sCx8-6C, e) cCx5-6C, f) pCx5-6C, g) sCx4, and h) sCx4-12C. Changes in fractional CF emission intensity (λ_{ex} = 492 nm, λ_{em} = 517 nm) were monitored in real time upon addition of varying concentrations of calixarenes, 0.125 μM polyLys, and TX-100 (for calibration) to 10.0 μM EYPC-LUVs⊃CF in 10 mM HEPES, 107 mM NaCl, pH 7.4, 25 °C.

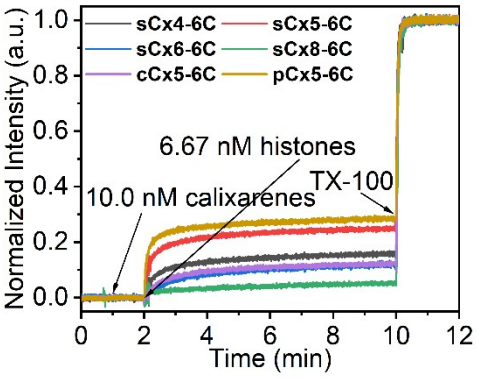

Figure S10. Changes in fractional CF emission intensity (λ_{ex} = 492 nm, λ_{em} = 517 nm) were monitored in real time upon addition of 10.0 nM calixarenes at 1 min, 6.67 nM histones at 2 min, and TX-100 (for calibration) at 10.0 min to 10.0 μM EYPC-LUVs⊃CF in 10 mM HEPES, 107 mM NaCl, pH 7.4, 25 °C.

5.3 NMR results of host-guest complexation

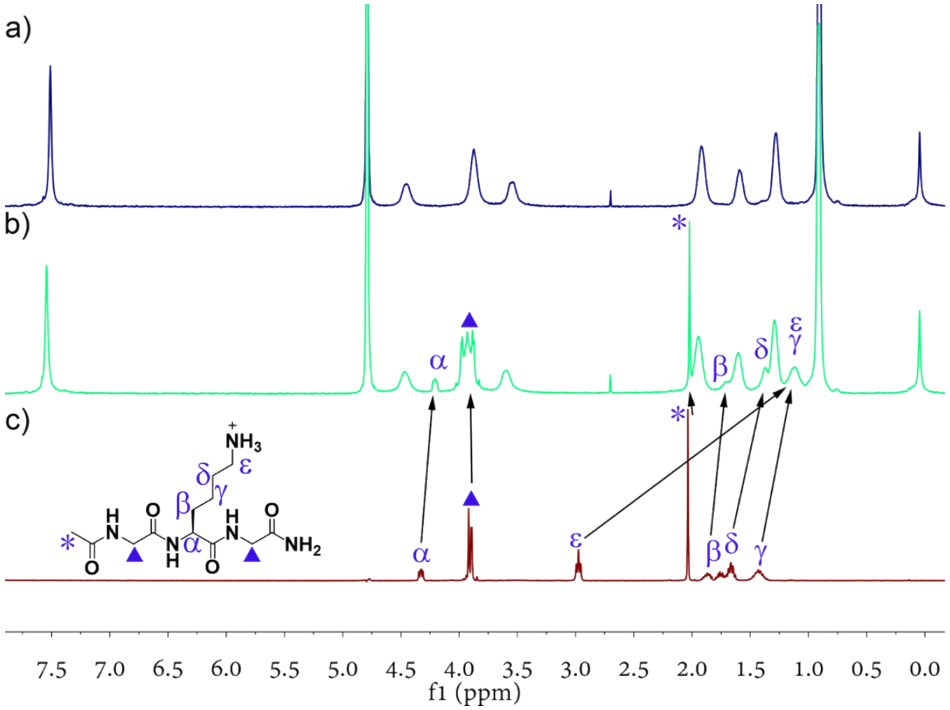

Figure S11. ^{1}H NMR spectra of a) sCx5-6C, b) the complex of sCx5-6C with Ac-GKG-NH_2, and c) Ac-GKG-NH_2 in D_2O, 400 MHz, 25 °C. The illustration shows the chemical structure of Ac-GKG-NH_2.

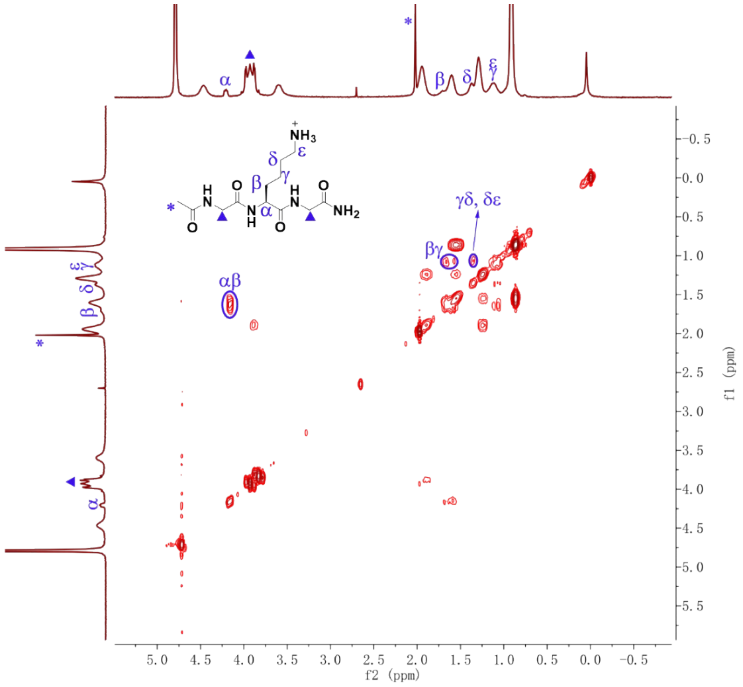

Figure S12. 2D COSY NMR spectrum of the complex of sCx5-6C with Ac-GKG-NH_2 in D_2O, 25 °C.

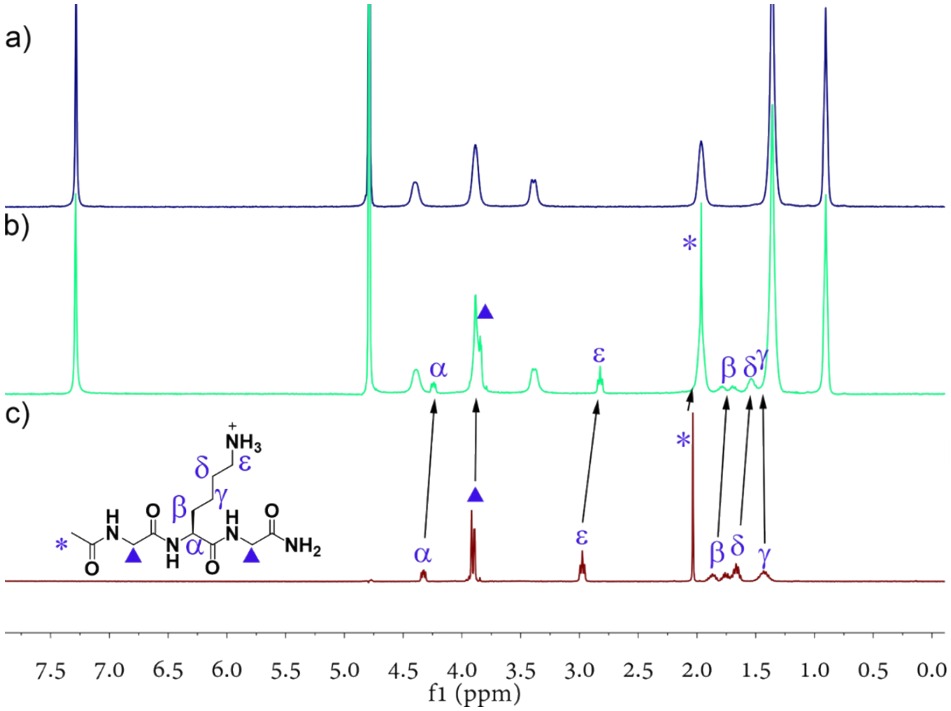

Figure S13. ^1H NMR spectra of a) sCx4-6C, b) the complex of sCx4-6C with Ac-GKG-NH_2, and c) Ac-GKG-NH_2 in D_2O, 400 MHz, 25 °C. The illustration shows the chemical structure of Ac-GKG-NH_2.

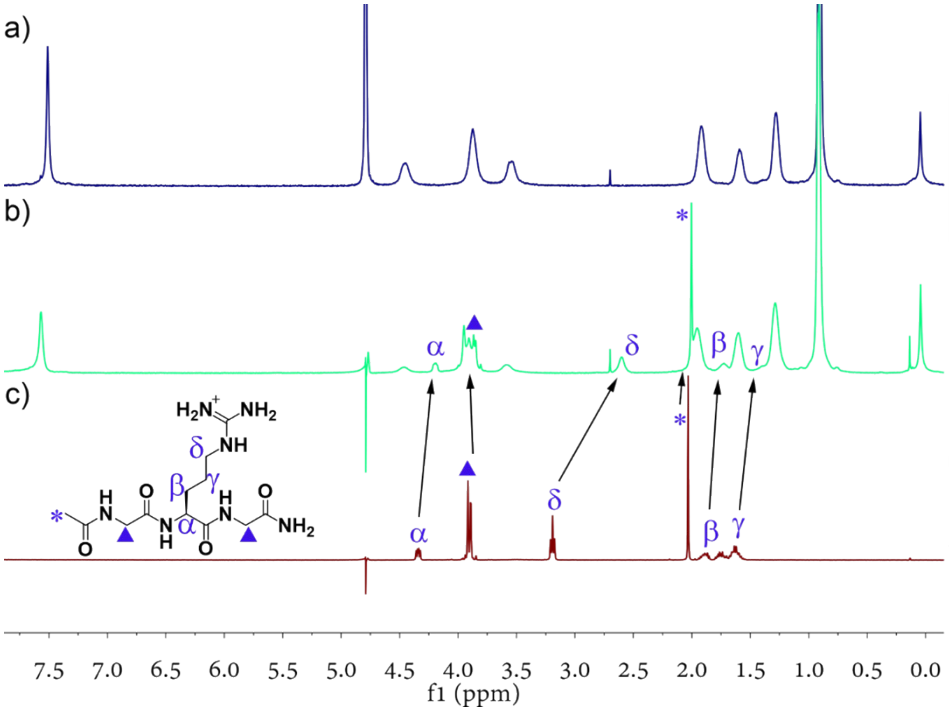

Figure S14. ^{1}H NMR spectra of a) sCx5-6C, b) the complex of sCx5-6C with Ac-GRG-NH_2, and c) Ac-GRG-NH_2 in D_2O, 400 MHz, 25 °C. The illustration shows the chemical structure of Ac-GRG-NH_2. The negative solvent peak is due to the phase distortion caused by water peak suppression.

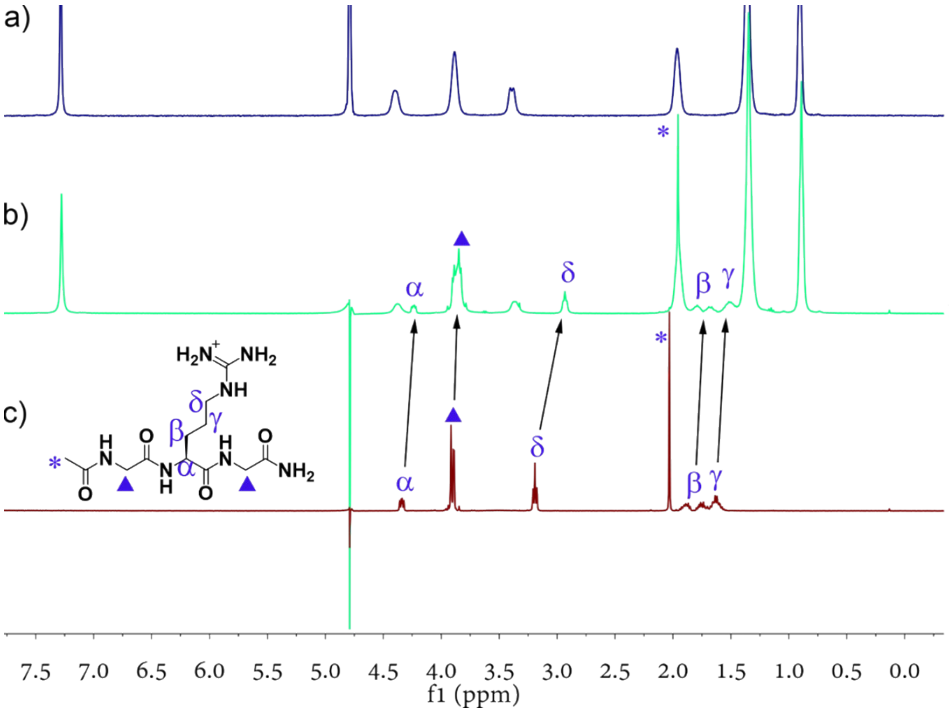

Figure S15. ^{1}H NMR spectra of a) sCx4-6C, b) the complex of sCx5-6C with Ac-GRG-NH_2, and c) Ac-GRG-NH_2 in D_2O, 400 MHz, 25 °C. The illustration shows the chemical structure of Ac-

GRG-NH_2. The negative solvent peak is due to the phase distortion caused by water peak suppression.

5.4 Results of fluorescence anisotropy

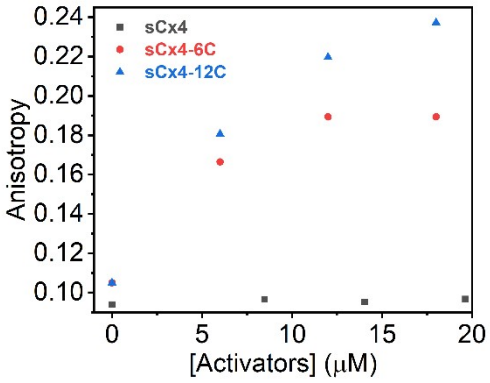

Figure S16. Fluorescence anisotropies of DPH (1.00 μM) entrapped in 50.0 μM EYPC-LUVs in the absence and presence of different concentrations of sCx4, sCx4-6C and sCx4-12C.

6. References

1 M.-X. Chen, T. Li, S. Peng and D. Tao, *New J. Chem.* 2016, **40**, 9923.

2 N. Basílio, L. Garcia-Rio and M. Martín-Pastor, *Langmuir* 2012, **28**, 2404.

3 Y.-C. Pan, A. Barba-Bon, H.-W. Tian, F. Ding, A. Hennig, W. M. Nau and D.-S. Guo, *Angew. Chem. Int. Ed.* 2021, **60**, 1875.

4 S. Shinkai, S. Mori, H. Koreishi, T. Tsubaki and O. Manabe, *J. Am. Chem. Soc.* 1986, **108**, 2409.

5 S. Sayin and M. Yilmaz, *Tetrahedron* 2016, **72**, 6528.

6 J. C. Stewart, *Anal. Biochem.* 1980, **104**, 10.

7 F. Perret, M. Nishihara, T. Takeuchi, S. Futaki, A. N. Lazar, A. W. Coleman, N. Sakai and S. Matile, *J. Am. Chem. Soc.* 2005, **127**, 1114.

8 M. Nishihara, F. Perret, T. Takeuchi, S. Futaki, A. N. Lazar, A. W. Coleman, N. Sakai and S. Matile, *Org. Biomol. Chem.* 2005, **3**, 1659.

9 S. Peng, A. Barba-Bon, Y.-C. Pan, W. M. Nau, D.-S. Guo and A. Hennig, *Angew. Chem. Int. Ed.* 2017, **56**, 15742.